International
Progress Report

IPR-04-38

Äspö Hard Rock Laboratory

Äspö Task Force

Application of FEGM and FERM to Task 6A, 6B and 6B2

Performance assessment modelling using site characterisation data

Yasuharu Tanaka

Central Research Institute of Electric Power Industry

August 2004

Svensk Kärnbränslehantering AB
Swedish Nuclear Fuel
and Waste Management Co
Box 5864
SE-102 40 Stockholm Sweden
Tel 08-459 84 00
+46 8 459 84 00
Fax 08-661 57 19
+46 8 661 57 19

Äspö Hard Rock
Laboratory

Report no.
IPR-04-38
No.
F65K
Author
Yasuharu Tanaka
Date
2004-08-11
Checked by
Date
Approved
Christer Svemar
Date
2004-11-19

Äspö Hard Rock Laboratory

Äspö Task Force

Application of FEGM and FERM to Task 6A, 6B and 6B2

Performance assessment modelling using site characterisation data

Yasuharu Tanaka

Central Research Institute of Electric Power Industry

August 2004

Keywords: Fracture modelling, Solute transport, Performance assessment, Tracer test

Abstract

In this report, we describe the result of our study in which we applied our numerical codes FEGM and FERM to Task 6A, Task 6B and Task 6B2 among the modelling issues of the Äspö Modelling Task Force. Task 6 seeks to provide a bridge between site characterization (SC) and performance assessment (PA) approaches to solute transport in fractured rock. Task 6A consists of modeling selected tracers used in the STT-1b test performed within the TRUE-1 program. Task 6B consists of modeling selected tracers used in the STT-1b test with new PA relevant boundary conditions and time scales. In Task 6B2, the boundary conditions are modified to produce flow and transport over a larger area of Feature A.

In this analysis, it was considered that Feature A was a single fracture and fault gouge was partially contained inside it. And Äspö diorite surrounding Feature A was considered to be altered in the vicinity of Feature A. In Feature A, the processes of advection, dispersion and surface related sorption of the tracers were considered. On the other hand, in the altered and unaltered Äspö diorite, the processes of matrix diffusion and sorption as well as advection and dispersion were considered. In fault gouge, only the process of matrix sorption was considered.

In this study, numerical codes based on the Galerkin finite element method, FEGM and FERM, were used for groundwater flow and solute transport, respectively.

The values of transport parameters such as surface related sorption coefficient and porosities, pore diffusivities and distribution coefficients of rock matrix given by SKB were generally used in this study. But the distribution coefficients of strontium and cobalt for fault gouge were calibrated through the simulations of STT-1b.

In each Task, at first, groundwater flow in Feature A and the surrounding rock matrix was calculated and next a numerical analysis for tracer migration was performed. The tracers modelled in the analysis were americium as well as iodine, strontium, cobalt and technetium that were actually used in STT-1b.

In Task 6A, the recovered mass flux decreased more rapidly after the peak than in Task 6B and 6B2. So relatively advection was prominent in Task 6A and matrix diffusion was prominent in Task 6B and 6B2. The significant technical issues in achieving Task 6A were estimation of transmissivity distribution and aperture of Feature A and sorption coefficients in gouge. On the other hand, the significant technical issues in achieving Task 6B and6B2 were estimation of sorption coefficients in altered rim and intact rock.

In order to improve the reliability of a performance assessment, it is very important how to estimate accurately the transport properties, especially surface and matrix sorption coefficients, from the results of in-situ tracer experiments and laboratory tests. In this study, the breakthrough curves obtained by using the one-dimensional model were very different from the ones by using the three-dimensional model. In case of performing a performance assessment by using a one-dimensional model, it is one of the significant problems to be solved how to find the value of dispersion length that produces the same calculated result as a three-dimensional model.

Sammanfattning

I denna rapport beskriver vi resultatet av vår studie i vilken vi applicerat våra numeriska program FEGM och FERM på Task 6A, Task 6B och Task 6B2 av modelleringsuppgifterna i Äspö Modelling Task Force. Task 6 syftar till att överbrygga gapet mellan platsundersöknings- och säkerhetsanalysansatser vad beträffar transport av lösta ämnen i berg. Task 6A består av modellering av ett urval av spårämnen som har använts i försöket STT-1b från TRUE-1 programmet. Task 6B består av modellering av försöket STT-1b med randvillkor som är relevanta för säkerhetsanalysförhållanden och –tidsskalor. I Task 6B2 modifieras randvillkoren för att ge strömning över ett större område av Feature A.

I denna analys betraktades Feature A som en enskild spricka som delvis är fylld med sprickfyllnadsmineral. Äspödioriten som omger sprickan betraktades som påverkad i närheten av Feature A. De processer som antagits försiggå i Feature A är advektion, dispersion och ytrelaterad sorption av spårämnen. I den påverkade såväl som i den opåverkade Äspödioriten har hänsyn tagits till matrisdiffusion och sorption liksom till advektion och dispersion. I sprickfyllnadsmineralen antogs endast matrisdiffusion.

De program som användes i studien, FEGM för grundvattenströmning och FERM för transport av lösta ämnen, bygger båda på Galerkins formulering av FinitaElementMetoden.

I allmänhet användes de värden på transportparametrarna, såsom ytsorptionskoefficienten, porositeten, pordiffusiviteten och fördelningskoefficienterna för bergmatrisen, som angivits av SKB. Fördelningskoefficienten för strontium och kobolt i sprickfyllnadsmineral togs dock fram genom kalibrering av modellen mot STT-1b försöket.

I varje uppgift beräknades först grundvattenströmningen varefter en numerisk analys av spårämnesmigrationen genomfördes. De spårämnen som modellerades i analysen var dels americium, dels jod, strontium, kobolt och teknetium som faktiskt användes i STT-1b.

I Task 6A minskade det uppsamlade massflödet efter passagen av toppen snabbare än i Task 6B och 6B2. Den viktigaste tekniska frågan som behandlades i Task 6A var uppskattningen av transmissivitetsfördelningen och sprickvidden i Feature A liksom sorptionskoefficienterna i sprickfyllnadsmineralen. I Task 6B och 6B2 var de mest signifikanta tekniska frågorna uppskattningen av sorptionskoefficienterna i den påverkade zonen och i det opåverkade berget.

Det är mycket viktigt, för att förbättra säkerhetsanalysens tillförlitlighet, att komma underfund med hur man från spårämnesförsök korrekt skall kunna uppskatta transportegenskaperna, särskilt för yt- och matrissorptionskoefficienter i fält och i laboratoriet. I denna studie skilde sig de genombrottskurvor som man fick vid endimensionell modellering markant från dem som erhölls med en tredimensionell modell. När man använder en endimensionell modell i en säkerhetsanalys ett av de väsentliga problemen som behöver lösas är att hitta ett värde på dispersionskoefficienten som producerar samma beräkningsresultat som en tredimensionell modell.

Executive summary

The Äspö Task Force is a forum for the organisations supporting the Äspö HRL project to interact in the area of conceptual and numerical modelling of groundwater flow and solute transport in fractured rock. Different experiments at the Äspö HRL are utilised to support the Modelling Tasks. Task 6 seeks to provide a bridge between site characterization (SC) and performance assessment (PA) approaches to solute transport in fractured rock.

In this report, we describe the result of our study in which we applied our numerical codes FEGM and FERM to Task 6A, Task 6B and Task 6B2 among the modelling issues of the Modelling Task Force. Task 6A consists of modeling selected tracers used in the STT-1b test performed within the TRUE-1 program. Task 6B consists of modeling selected tracers used in the STT-1b test with new PA relevant boundary conditions and time scales. In Task 6B2, the boundary conditions are modified to produce flow and transport over a larger area of Feature A.

In this analysis, it was considered that Feature A was a single fracture and fault gouge was partially contained inside it. And Äspö diorite surrounding Feature A was considered to be altered in the vicinity of Feature A. In Feature A, the processes of advection, dispersion and surface related sorption of the tracers were considered. On the other hand, in the altered and unaltered Äspö diorite, the processes of matrix diffusion and sorption as well as advection and dispersion were considered. In fault gouge, only the process of matrix sorption was considered.

In this study, numerical codes based on the Galerkin finite element method, FEGM and FERM, were used for groundwater flow and solute transport, respectively. In this study, a rock block on only one side of Feature A was modelled. In Task 6A, the modelled region was a rectangular prism with a base 30 m x 30 m and a thickness of 0.1 m. In Task 6B, the same model as Task 6A was used for groundwater flow but a smaller model was used for solute transport. In task 6B2, the modelled region was a rectangular prism with a base 20 m x 15 m and a thickness of 0.1 m bounded by two fractures X and Y.

Transmissivity was assumed to distribute in Feature A with a spatial correlation. And the distribution of transmissivity in Feature A was identified on the basis of the data of drawdown during the several tracer tests. The fracture aperture was assumed to be constant throughout Feature A. And the value of aperture was identified through the numerical simulation of the tracer tests, STT-1b.

The values of transport parameters such as surface related sorption coefficient and porosities, pore diffusivities and distribution coefficients of rock matrix given by SKB were generally used in this study. But the distribution coefficients of strontium and cobalt for fault gouge were calibrated through the simulations of STT-1b.

In each Task, at first, groundwater flow in Feature A and the surrounding rock matrix was calculated and next a numerical analysis for tracer migration was performed. The tracers modelled in the analysis were americium as well as iodine, strontium, cobalt and technetium that were actually used in STT-1b.

In Task 6A, the calculated head difference between pumping and tracer injection sections is 3.1 meters smaller than the measured one. The more strongly adsorptive the tracer was, the slower its breakthrough time was. The breakthrough time for recovery of 50 %, t_{50}, of the pulse injection of the non-sorbing tracer, iodine, was $1.95 \cdot 10^{-3}$ years after the tracer test began. On the other hand, t_{50} of the most strongly adsorptive tracer, americium, was 3.64 years after. The finish time of calculation was 10 years after the tracer test began and at the time the total recovery rates of the strongly adsorptive tracers, technetium and americium, were below 95 %. The more strongly adsorptive the tracer was, the smaller its maximum release rate was. The maximum release rate of the pulse injection of iodine was $1.74 \cdot 10^{4}$ larger than the one of americium.

In Task 6B, the proportion of the calculated hydraulic gradient between the pumping and tracer injection sections to the one in Task 6A was 0.105 %. The calculated breakthrough time for recovery of 50 %, t_{50}, of the pulse injection of iodine was 0.93 years after the tracer test began. On the other hand, t_{50} of americium was $2.14 \cdot 10^{4}$ years after. The finish time of calculation was 10^{7} years after the tracer test began and at the time the total recovery rate of only americium was below 95 %. The maximum release rate of iodine for a Dirac pulse injection was $2.35 \cdot 10^{4}$ larger than the one of americium.

In Task 6B2, the overall hydraulic gradient between the two intersecting fractures was 0.1 %. In the tracer migration analysis, not only a 3-D model but also a 1-D model were used. When a three-dimensional model was used, the breakthrough time for recovery of 50 %, t_{50}, of the pulse injection of iodine was 1.91 years after the tracer test began and t_{50} of americium was $5.5 \cdot 10^{4}$ years after. And the maximum release rate was the largest, $4.28 \cdot 10^{-1}$ year^{-1}, in iodine and the smallest, $1.51 \cdot 10^{-5}$ year^{-1}, in americium. On the other hand, when a one-dimensional model was used, t_{50} of iodine and americium were 1.33 years and $1.78 \cdot 10^{4}$ years after, respectively. And the maximum release rate was the largest, $7.84 \cdot 10^{-1}$ year^{-1}, in iodine and the smallest, $5.71 \cdot 10^{-5}$ year^{-1}, in americium.

In Task 6A, the recovered mass flux decreased more rapidly after the peak than in Task 6B and 6B2. So relatively advection was prominent in Task 6A and matrix diffusion was prominent in Task 6B and 6B2. The significant technical issues in achieving Task 6A were estimation of transmissivity distribution and aperture of Feature A and sorption coefficients in gouge. On the other hand, the significant technical issues in achieving Task 6B and6B2 were estimation of sorption coefficients in altered rim and intact rock.

In order to improve the reliability of a performance assessment, it is very important how to estimate accurately the transport properties, especially surface and matrix sorption coefficients, from the results of in-situ tracer experiments and laboratory tests. And we need to take the irreversible adsorption process into consideration to predict the migration of some radionuclides such as cobalt.

In this study, the breakthrough curves obtained by using the one-dimensional model were very different from the ones by using the three-dimensional model. In case of performing a performance assessment by using a one-dimensional model, it is one of the significant problems to be solved how to find the value of dispersion length that produces the same calculated result as a three-dimensional model.

Contents

List of tables

List of figures

1 Introduction

The scenario of released radionuclides from engineered barriers to the biosphere along the groundwater flow pathways is critical to the execution of high-level radioactive waste disposal. CRIEPI has been developing numerical codes for the analyses of groundwater flow and solute transport in rock formation to assess the safety of disposal facilities of radioactive wastes.

The Äspö Hard Rock Laboratory (HRL) was constructed by the Swedish Nuclear Fuel and Waste Management Co. (SKB) near Oskarshamn, southeastern Sweden, to investigate high-level waste disposal in a deep geological formation. Several international organizations are participating in collaborative projects. One of these projects, Task Force on Modelling of Groundwater Flow and Transport of Solutes, is a forum supporting the Äspö Hard Rock Laboratory to interact in the area of conceptual and numerical modelling of groundwater flow and solute transport in fractured rock. CRIEPI has participated in the Modelling Task Force since 1992.

In this report, we describe the result of our study in which we applied our numerical codes FEGM and FERM to Task 6A, Task 6B and Task 6B2 among the modelling issues of the Modelling Task Force.

2 Modelling Tasks

The Äspö Task Force is a forum for the organisations supporting the Äspö HRL project to interact in the area of conceptual and numerical modelling of groundwater flow and solute transport in fractured rock (SKB, 2003). In particular, the Task Force shall propose, review, evaluate and contribute to such work in the project. The Task Force shall interact with the principal investigators responsible for carrying out experimental and modelling work for Äspö HRL of particular interest for the members of the Task Force.

Much emphasis is put on building of confidence in the approaches and methods in use for modelling of groundwater flow and migration in order to demonstrate their use for performance and safety assessment.

Different experiments at the Äspö HRL are utilised to support the Modelling Tasks. The past modelling issues were as follow:

Task 1: Long term pumping and tracer experiments (LPT-2).

Task 2: Scooping calculations for some of the planned detailed scale experiments at the Äspö site.

Task 3: The hydraulic impact of the Äspö tunnel excavation.

Task 4: The Tracer Retention and Understanding Experiment (TRUE), 1st stage.

Task 5: Coupling between hydrochemistry and hydrogeology.

Task 6 seeks to provide a bridge between site characterization (SC) and performance assessment (PA) approaches to solute transport in fractured rock. In Task 6 both PA-type and SC-type models will be applied to tracer experiments considering both the experimental boundary conditions and boundary conditions for a PA scale. The modelers were requested first to implement their models such that they can reproduce the results from relevant TRUE-1 *in situ* tracer experiments. And they were allowed to make appropriate assumptions for PA modeling, while continuing to honor the *in situ* tracer experiment results.

The outlines of Task 6A, 6B and 6B2 are as follow (Selroos *et al*., 2001 and Elert *et al*., 2001).

2.1 Task 6A

The task consists of modeling selected tracers used in the STT-1b test performed within the TRUE-1 program. The test was made between packed off boreholes penetrating a water-conducting geological feature with a simple structure (Feature A), *see* Figure 2-1.

The purpose of Task 6A is to provide a common basis for future comparison of the modeling carried out within Task 6. The task is defined so that both PA and SC type models can be used.

The tracer test was performed using a radially converging flow geometry with pumping in borehole section KXTT3 R2 and injection of tracer in borehole section KXTT1 R2, both penetrating Feature A (Anderson *et al*., 1999). The travel distance between the boreholes was 5.03 meters. The injection section was equipped with a circulation system where a solution containing twelve different tracers were injected as a finite pulse with a duration of 4 hours. Four non-sorbing (Uranine, HTO, ^{82}Br, ^{131}I) and six weakly to moderately radioactive sorbing tracers (^{22}Na, ^{42}K, ^{85}Sr, ^{99m}Tc, ^{58}Co and ^{86}Rb) were used. After four hours of injection the tracer solution was exchanged in two steps with unlabelled water. The first exchange lasted for 60 minutes and the second exchange, 100 minutes after the end of the first one, lasted for 25 minutes. The pumping in the withdrawal section (KXTT3 R2) was 0.4 l/min.

The tracer test STT-1b was previously modeled in Task 4E. The modelers were provided with site characterization data, data from preliminary tracer tests with non-sorbing tracers, laboratory measurements of retention parameters (De, Ka and Kd) and were asked to predict the tracer breakthrough. The predictions for the sorbing tracer using the laboratory measurements of retention parameters generally underestimated the breakthrough time. In order to have an acceptable fit to the experimental data, the modelers needed to modify their models and/or adapt the laboratory data.

2.2 Task 6B

The task consists of modeling selected tracers used in the STT-1b test performed within the TRUE-1 program with new PA relevant boundary conditions and time scales. The purpose of Task 6B is to identify and understand differences between the use of SC-type and PA-type models, and to study the influence of various assumptions made for PA calculation concerning extrapolation in time. The task is defined so that both PA and SC type models can be used.

When going from SC-scale to PA-scale the modelers are expected to adapt their models in such way that the transport and retention processes are described in a relevant way.

The STT-1b test is adjusted to PA-conditions with the following assumptions:

1. In the TRUE-1 tracer experiments the gradient between the injection and pumping sections was in the order of 1, while in natural conditions a gradient could be expected in the order of 0.1%. Due to the change in gradient a water flow rate 1000 times lower than in Task 6A is to be modeled. This could be achieved by different means, e.g. by changing the gradient or the pumping rate.

2. The same flowpath is assumed for Task 6B as in Task 6A, i.e. passive injection in KXTT1 R2 and withdrawal in section KXTT3 R2.

3. The background head field observed during the TRUE-1 experiment should not be used, since it is assumed that the Äspö tunnel no longer causes a drawdown in Feature A.

2.3 Task 6B2

Task 6B2 is focused on transport in Feature A. In this task, the boundary conditions are modified to produce flow and transport over a larger area of Feature A than in Task6B. The situation envisaged is of a PA-type where there is no tunnel causing drawdown. Instead the water flow is governed by small natural gradients. In the modelling task, the water flow in Feature A is assumed to be governed by the head difference between two parallel fractures (X and Y) intersecting Feature A. A graphical representation of the geometry is given in Figure 2-2.

The hydrological boundary conditions are constant heads at the intersecting fractures. The head difference should be 0.015 metres giving a gradient of 0.1%. The flow will follow the general direction of the flow path used in STT-1b, i.e. from KXTT1 to KXTT3. However, in this case no pumping will occur in KXTT3.

The input boundary is no longer a point source. Injection is assumed to occur along a 2 metre long line source overlapping the position of borehole section KXTT1 R2. The distance from the intersecting Fracture X to the injection line is 5 metres. Tracer is collected in the upper intersecting Fracture Y, situated a distance of 10 meters from the injection section. The tracers to be modeled for Task 6B2 are iodine, strontium, cobalt, technetium and americium.

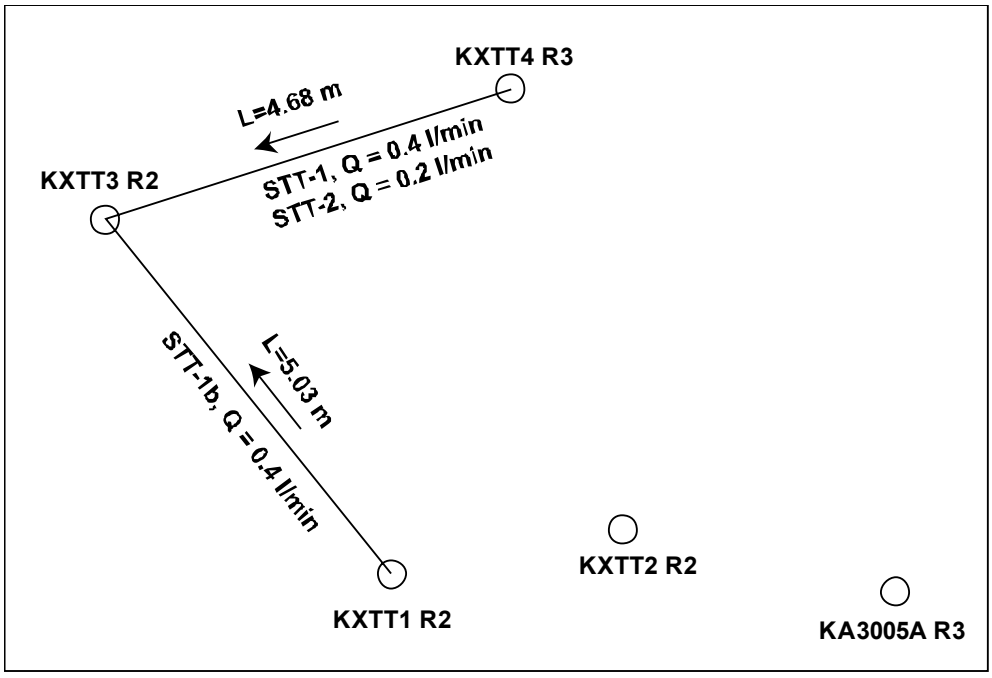

Figure 2-1. *Test geometry, pumping flow rates (Q) and borehole intersection pattern with Feature A for the tracer tests STT-1, STT-1b and STT-2 (Selroos et al., 2001).*

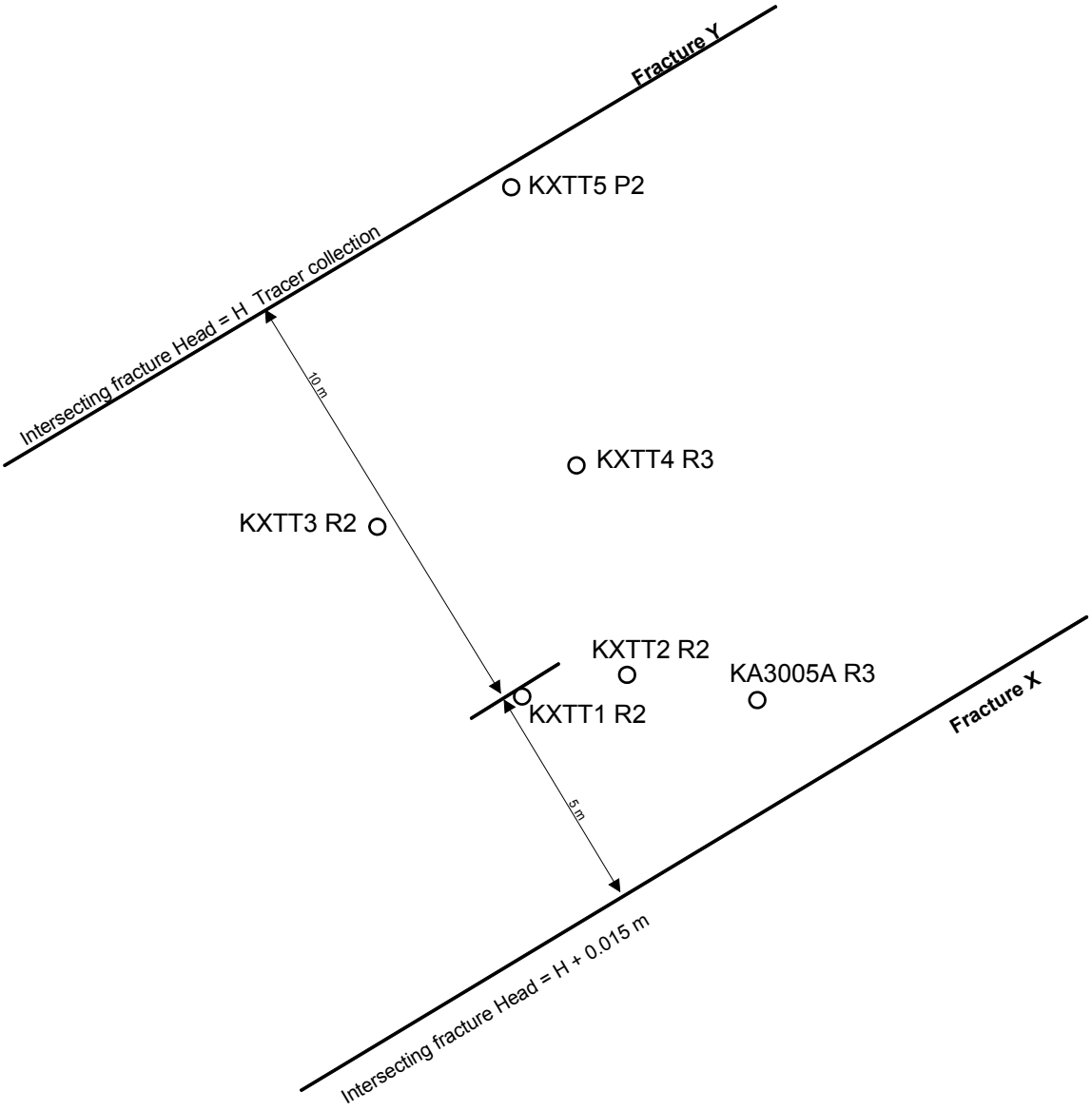

Figure 2-2. *Geometry of Task 6B2. Injection at line source at KXTT1 R2. Tracer collection at Fracture Y. (Elert et al., 2001).*

3 Model description

3.1 Geometrical description

In this analysis, it was considered that Feature A was a single fracture and fault gouge was partially contained inside it. And it was assumed that Feature A was hydraulically isotropic and its aperture was constant throughout the fracture plane. Äspö diorite surrounding Feature A was considered to be altered in the vicinity of Feature A.

3.2 Processes considered

In Feature A, the processes of advection, dispersion and surface related sorption of the tracers were considered, cf. Figure 3-1. On the other hand, in the altered and unaltered Äspö diorite, the processes of matrix diffusion and sorption as well as advection and dispersion were considered.

In fault gouge, only the process of matrix sorption was considered. And the amounts of the tracers adsorbed on fault gouge were assumed to exist in equilibrium with the tracer concentration of the groundwater in Feature A all the time.

3.3 Numerical model

3.3.1 Groundwater flow

In this study, a numerical code based on the Galerkin finite element method, FEGM (Kawanishi, 1987), was used for groundwater flow. FEGM has been developed by CRIEPI on basis of a numerical code, FEMWATER (Yeh *et al*., 1979).

The basic equations for groundwater flow considered in FEGM are composed of the continuum equation and Darcy's law. These equations are discretized to a finite element.

The continuum equation for groundwater flow :

$$\left(\theta\beta + \frac{\theta}{\phi}\alpha + \frac{\partial\theta}{\partial h}\right)\frac{\partial h}{\partial t} + \frac{\partial}{\partial x_i}V_i + Q = 0 \qquad 3\text{-}1$$

where θ is the volumetric water content, β the compressibility of water, ϕ the porosity, α the compressibility of media, h the pressure head, t the time, V_i the Darcy's velocity, x_i the coordinate and Q the sink/source term.

Darcy's law:

$$V_i = -k_r \cdot K \frac{\partial H_D}{\partial x_i} = -k_r \cdot K \left(\frac{\partial h}{\partial x_i} + \frac{\rho}{\rho_0} \frac{\partial z}{\partial x_i} \right) \quad 3\text{-}2$$

$$H_D = h + \frac{1}{\rho_0} \int \rho dz \approx h + \frac{\rho}{\rho_0} z \quad 3\text{-}3$$

where k_r is the relative permeability, K the hydraulic conductivity tensor, H_D the hydraulic head, ρ the density, ρ_o the density of reference water and z the vertical coordinate.

In this study, a rock block on only one side of Feature A was modelled. The finite element mesh used for the groundwater flow analyses of Task 6A and 6B is shown in Figure 3-2. The modelled region was a rectangular prism with a base 30 m x 30 m and a thickness of 0.1 m. On the other hand, the finite element mesh shown in Figure 3-3 was used for the groundwater flow analyses of Task 6B2. The modelled region was a rectangular prism with a base 20 m x 15 m and a thickness of 0.1 m bounded by two fractures X and Y. In both meshes, Feature A and rock matrix were modelled by plane elements with thickness of half the aperture of Feature A and hexahedral elements, respectively.

In Task 6A, the hydraulic heads on the boundary planes intersecting perpendicularly to Feature A were calibrated, *see* 3.5.2, and fixed. In Task 6B, the hydraulic head was fixed at a same value at any point on those boundary planes. In task 6B2, the hydraulic head on the boundary plane expressing the fracture X was set 0.015 m higher than the one on the boundary plane expressing the fracture Y and no water flow was assumed to cross the two remaining boundary planes intersecting perpendicularly to Feature A. And in all these Tasks, the boundary plane expressing the center plane of Feature A and the boundary plane opposite to Feature A were constrained as no flux boundaries.

3.3.2 Solute transport

In this study, a numerical code based on the Galerkin finite element method, FERM (Kawanishi, 1987), was used for solute transport. FERM has been developed by CRIEPI on basis of a numerical code, FEMWASTE (Yeh *et al*., 1981).

The governing equation for solute transport considered in FERM is the advection-dispersion equation. The equation is discretized to a finite element in a fashion similar to the groundwater flow.

The governing equation for solute transport :

$$(\theta+\rho_b K_d)\frac{\partial}{\partial t}C+\left\{\frac{\partial\theta}{\partial t}+\alpha(\theta+\rho_b K_d)\frac{\partial h}{\partial t}\right\}C$$
$$-\frac{\partial}{\partial x_i}\theta D_{ij}\frac{\partial}{\partial x_j}C+\frac{\partial}{\partial x_i}V_i C+\{\lambda(\theta+\rho_b K_d)+(K_w\theta+K_s\rho_b K_d)\}C+M=0 \qquad 3\text{-}4$$

$$\theta D_{ij}=\alpha_T\|V\|\delta_{ij}+(\alpha_L-\alpha_T)\frac{V_i V_j}{\|V\|}+D_m\tau\theta\delta_{ij} \qquad 3\text{-}5$$

where ρ_b is the bulk density of media, K_d the distribution coefficient, C the concentration of solute, λ the decay constant, K_w the decomposition rate constant in a liquid phase, K_s the decomposition rate constant in a solid phase, M the source term, α_L the longitudinal dispersion length, α_T the transverse dispersion length, D_m the molecular diffusion and τ the tortuosity.

In this study, the following equation was used for solute transport in Feature A.

$$b\left\{F+\frac{2FK_a}{b}+(1-F)\rho_{bg}K_{dg}\right\}\frac{\partial}{\partial t}C-\frac{\partial}{\partial x_i}bFD_{ij}\frac{\partial}{\partial x_j}C+\frac{\partial}{\partial x_i}bV_i C+M=0 \qquad 3\text{-}6$$

where b is the aperture of Feature A, K_a the surface related sorption coefficient, ρ_{bg} the bulk density of fault gouge, K_{dg} the distribution coefficient for fault gouge and F the degree of separation of a fracture defined by the following equation.

$$F=\frac{\text{open surface area of a fracture}}{\text{total surface area of a fracture}} \qquad 3\text{-}7$$

On the other hand, equation 3-4 was used for solute transport in rock matrix.

In Task 6A, the same finite element mesh as for the groundwater flow analysis was used for the solute transport analysis. But in Task 6B, the solute transport was analysed using the smaller finite element mesh on the basis of the result of the groundwater flow analysis, *see* Figure 3-2. In Task 6B2, the solute transport analysis was performed using not only the same three-dimensional finite element mesh as for the groundwater flow analysis but also a one-dimensional finite element mesh shown in Figure 3-4. The processes considered in the one-dimensional model were advection, dispersion and surface sorption in Feature A, matrix sorption for fault gouge and matrix sorption and diffusion to only the direction perpendicular to Feature A in the altered and unaltered Äspö diorite.

Throughout Task 6A, 6B and 6B2, the gradient of tracer concentration was assumed to be zero on all the boundary planes.

3.4 Parameters

Transmissivity was assumed to distribute in Feature A with a spatial correlation. And the distribution of transmissivity in Feature A was identified on the basis of the data of drawdown during the several tracer tests, *see* 3.5.1.

The fracture aperture was assumed to be constant throughout Feature A. And the value of aperture was identified through the numerical simulation of the tracer tests, STT-1b, *see* 3.5.4. The degree of separation of Feature A was assumed to be 0.5, *see* equation 3-7.

The total thickness of Feature A including altered Äspö diorite is varying between 0.05 and 0.09 m (Winberg *et al*., 2000). Therefore we set a 0.035 m thick block of altered diorite on each side of Feature A so that the total thickness of Feature A was 0.07 m, *see* Table 3-1. Besides a 0.065 m thick block of unaltered diorite was given on each outer side of the altered diorite. The hydraulic conductivity of the altered and unaltered diorite was assumed to be $1 \cdot 10^{-10}$ m/sec. Porosities of the altered and unaltered Äspö diorite and the fault gouge were assumed to be 0.006, 0.003 and 0.10, respectively (Selroos *et al*., 2001), *see* Table 3-2.

The longitudinal and transverse dispersion lengths were assumed to be one-tenth and one-hundredth of the distance between the tracer injection and recovery points, respectively, *see* Table 3-3. In the tracer test, STT-1b, the distance between the tracer injection and recovery borehole sections was 5.03 meters. Therefore, in Task 6A and Task 6B, we used 0.5 m and 0.05 m as the longitudinal and transverse dispersion lengths, respectively. On the other hand, the distance between the tracer injection section and Fracture Y where the tracers were collected was 10 m. Accordingly in Task 6B2, we used 1.0 m and 0.1 m as the longitudinal and transverse dispersion lengths, respectively.

The sorption and diffusivity data for tracers used in this study are shown in Table 3-4 to 3-6. The distribution coefficients of strontium and cobalt for altered rim and intact rock were quoted from Byegård *et al*., 2001. And the distribution coefficients of technetium and americium for altered rim and intact rock were quoted from Selroos J-O *et al*., 2001. We did not have any information on the distribution coefficients for fault gouge. Therefore the distribution coefficients of strontium and cobalt for fault gouge were calibrated through the simulations of STT-1b, *see* 3.5.5. The calibrated K_d-values of strontium and cobalt for fault gouge were several times larger than the K_d-values for altered rim and intact rock. Accordingly, not only the same values as for altered rim and intact rock but also ten times larger values were used as the K_d-values of technetium and americium for fault gouge in this study. The K_a-value of strontium was quoted from the Modelling Input Data Set, MIDS (Winberg et al., 2000) and the K_a-values of other radionuclides were quoted from Selroos J-O *et al*., 2001. The pore diffusivities of the tracers for the altered and unaltered Äspö diorite were quoted from MIDS (Winberg *et al*., 2000).

The density of the water was assumed to be 1005 kg/m^3.

3.5 Model calibration and development

3.5.1 Transmissivity in Feature A

The distribution of transmissivity in Feature A was was identified on the basis of the data of drawdown at the borehole sections intersecting Feature A during the four tracer tests, DP-1, DP-4, RC-2 and STT-1b.

The identification was performed according to the following procedure.

1) Give the values of transmissivity at the borehole sentions intersecting Feature A.
2) Calculate the average and varience of the values.
3) Estimate the distribution of transmissivity in Feature A by kriging on the basis of the values at the borehole sections.
4) Calculate the drawdowns at the borehole sections during the tracer tests.
5) Calculate the sum of the squares of normalized errors between the calculated and measured drawdowns, S_d, defined by the following equation.

$$S_d = \sum_{i,j} \left(\frac{\Delta h_{cj}^{\ i} - \Delta h_{mj}^{\ i}}{\Delta h_{mj}^{\ i}} \right)^2 \qquad 3\text{-}8$$

where $\Delta h_{mj}^{\ i}$ is the measured drawdown at the j-th borehole section during i-th tracer tests and $\Delta h_{cj}^{\ i}$ the calculated drawdown.

The transmissivity values at the borehole sections were changed by the method of trial and error and the procedure from 2) to 5) was repeated till the sum of the squares of normalized errors became sufficiently small. However, the transmissivity value at KA3005A R3 was fixed at the initial value, $4.20 \cdot 10^{-8}$ m^2/sec.

The values obtained from the flow and pressure build–up tests (Winberg *et al*., 2000) were chosen as the initial values of transmissivity at the five borehole sections

The exponential model was selected for the variogram (Delhomme, 1976).

$$\gamma(h) = \omega\{1 - \exp(-h/a)\} \qquad 3\text{-}9$$

where ω is the variance, h the distance and a the correlation length. The correlation length was assumed to be 0.4 m (Abelin *et al*., 1990).

The identified values of transmissivity at the borehole sections are shown in Table 3-7. And the distribution of transmissivity which has been estimated by kriging on the basis of the values is shown in Figure 3-5.

3.5.2 Hydraulic Boundary Condition

The hydraulic heads were fixed on the surrounding boundaries of the model as mentioned in 3.3. The hydraulic heads on the boundaries were identified so that the sum of the squares of normalized errors between the calculated heads and the observed ones at the five borehole sections prior to the STT-1b test, S_h, would be minimal.

$$S_h = \sum_{i=1}^{5} \left(\frac{h^i_{cal} - h^i_{obs}}{h^i_{obs}} \right)^2 \qquad 3\text{-}10$$

where h^i_{obs} is the observed hydraulic head at the i-th section prior to the STT-1b tracer test and h^i_{cal} the calculated one. The identified parameters were the hydraulic head at the point A, h_A, the magnitude of the average hydraulic gradient, I, and the angle between the direction of the average hydraulic gradient and the side AB, θ, *see* Figure 3-6. Table 3-8 gives the identified values of these parameters.

3.5.3 Mass Flux at Injection Section

The fluid flux through the tracer injection section, Q_{bh}, is obtained theoretically by the following equation (Winberg, 1996 and Andersson, 1996).

$$Q_{bh} = -\frac{V}{t} ln(C / C_0) - Q_{sam} \qquad 3\text{-}11$$

where V is the volume of the tracer injection section, t the elapsed time, C_0 the initial concentration of the tracer in the injection section, C the concentration at the time t and Q_{sam} the sampling flow rate.

The measured concentrations of Uranine at the injection section during STT-1b and the straight line for approximation are shown in Figure 3-7. By substituting the value of the slope of the straight line into equation 3-11, the fluid flux through the tracer injection section, KXTT1 R2, was estimated to be 58.0 ml/hour.

The product of the tracer concentration and the fluid flux was used as the mass flux of the tracer injected into Feature A for the tracer migration analysis in Task 6A.

3.5.4 Fracture aperture

In this study, aperture was assumed to be uniform through Feature A and the value of aperture was calibrated through a simulation of transport of iodine during STT-1b. The breakthrough curve at the pumping section was calculated for different aperture values. The breakthrough curve of the best-fit run is shown in Figure 3-8. As a result, aperture of Feature A was estimated to be 1.68 mm.

3.5.5 Distribution coefficient for fault gouge

The distribution coefficients of strontium and cobalt for fault gouge were calibrated through the simulations of STT-1b. The breakthrough curves of strontium and cobalt at the pumping section were calculated for different K_d-values. The breakthrough curves of the best-fit runs are shown in Figure 3-9 and 3-10. As a result, distribution coefficients of strontium and cobalt for fault gouge was estimated to be $2.0 \cdot 10^{-4}$ and $1.2 \cdot 10^{-2}$, respectively.

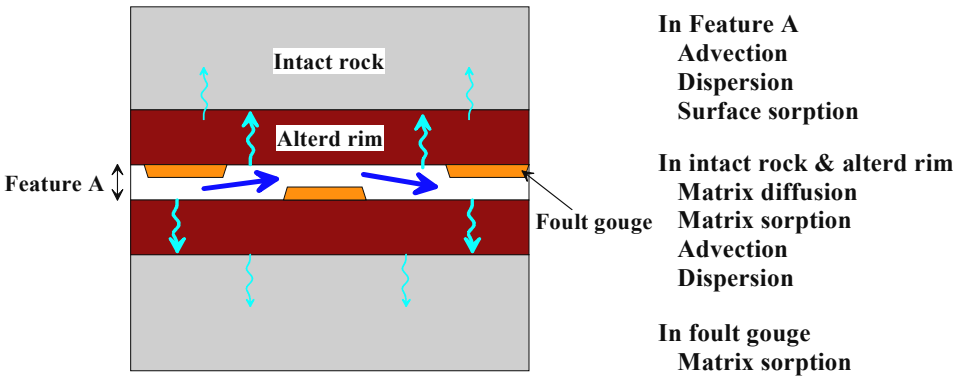

Figure 3-1. *Schematic view of the geometry and process considered in the analysis.*

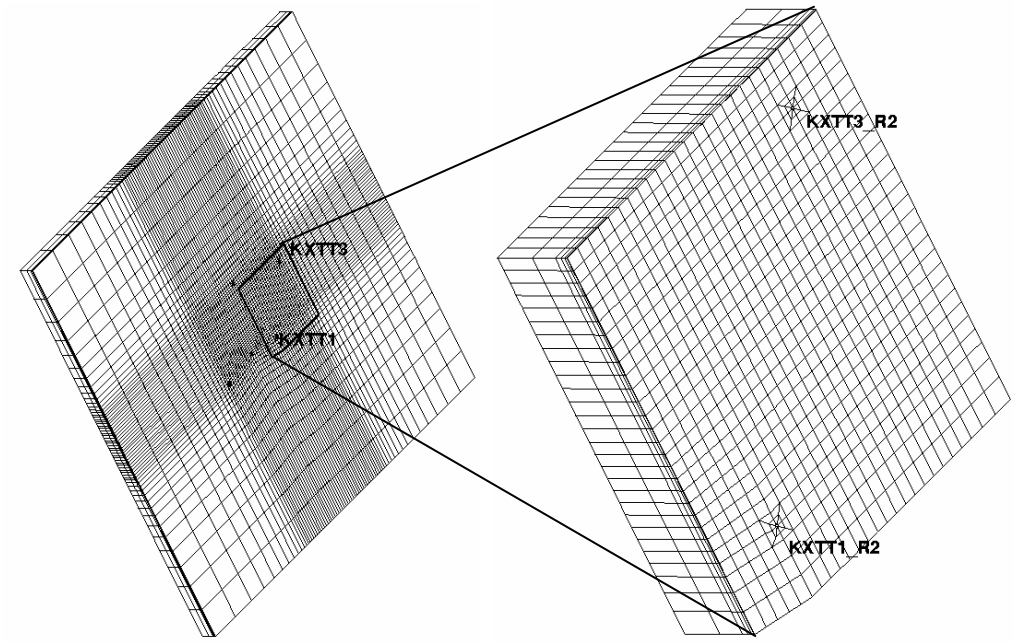

Figure 3-2. *Three-dimensional finite element mesh (left) used for the groundwater flow analyses of Task 6A and 6B and the solute transport analysis of Task 6A. And one (right) used for the solute transport analysis of Task 6B.*

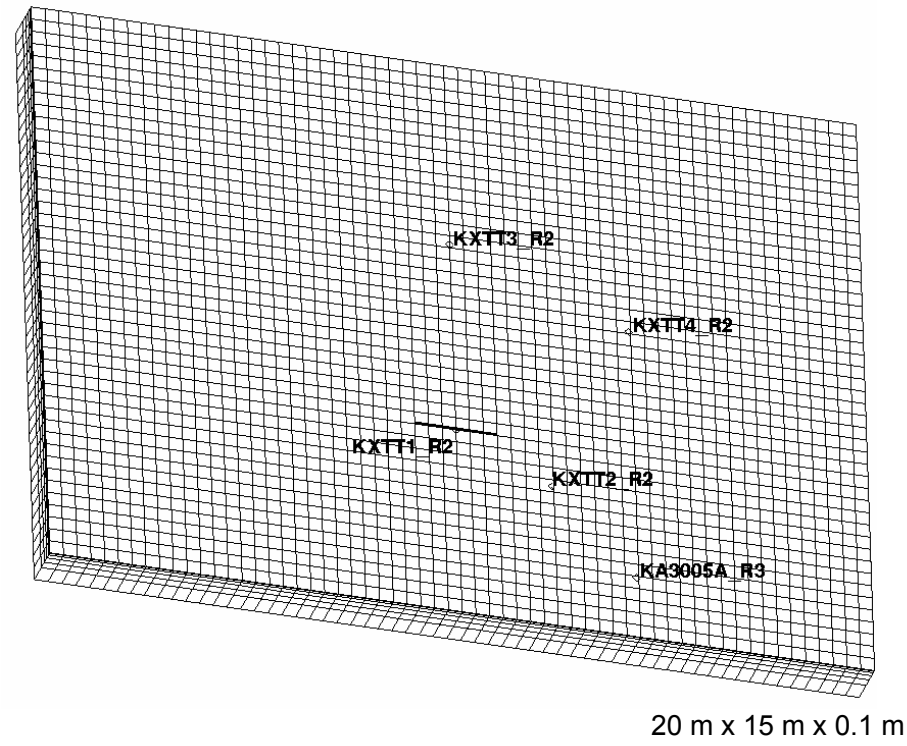

Figure 3-3. *Three-dimensional finite element mesh used for the groundwater flow and solute transport analyses of Task 6B2.*

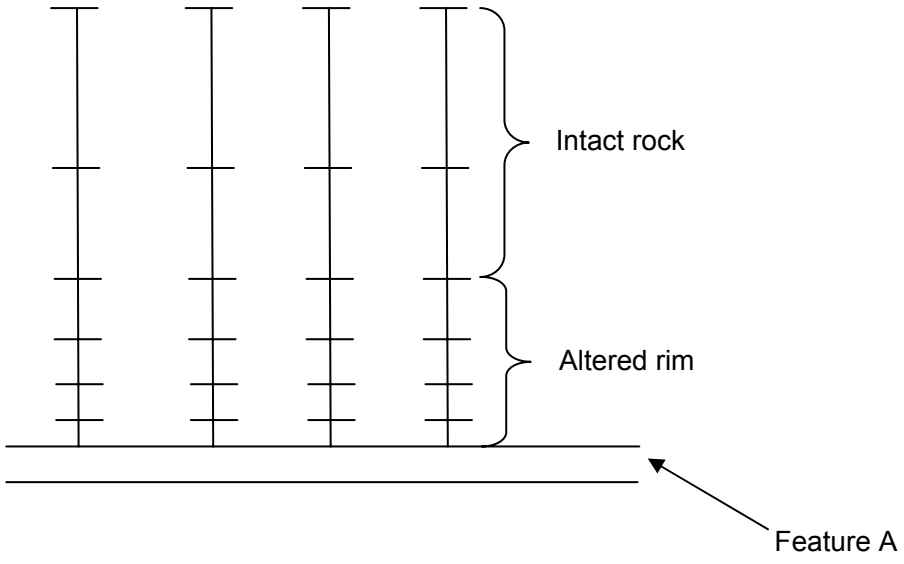

Figure 3-4. *One-dimensional finite element mesh used for the solute transport analysis of Task 6B2.*

Table 3-1. Thickness and hydraulic conductivity of surrounding rocks used in this study.

	Thickness (m)	Hydraulic conductivity (m/sec)
Altered rim	0.035	$1.0 \cdot 10^{-10}$
Intact rock	0.065	$1.0 \cdot 10^{-11}$

Table 3-2. Porosities of rock materials used in this study.

	Porosity (-)
Altered rim	0.006
Intact rock	0.003
Fault gouge	0.10

Table 3-3. Dispersion length used in this study. The same values were used for Feature A and rock matrix.

	Task 6A	Task 6B	Task 6B2
Longitudinal dispersion length, α_L, (m)	0.5	0.5	1.0
Transverse dispersion length, α_T, (m)	0.05	0.05	0.1

Table 3-4. Sorption and diffusivity data for tracers in alterd rim for Task 6A, 6B and 6B2.

Tracer	Matrix sorption coefficient K_d (m^3/kg)	Surface sorption coefficient K_a (m)	Effective matrix diffusivity D_e (m^2/s)
I	0	0	1.25E-13
Sr	7.75E-5*)	8.00E-6	6.00E-14
Co	2.50E-3*)	8.00E-3	4.35E-14
Tc	0.2**)	0.2	6.00E-14
Am	0.5**)	0.5	6.00E-14

*) from Byegård *et al*., 2001
**) from Selroos J-O *et al*., 2001

Table 3-5. Sorption and diffusivity data for tracers in intact rock for Task 6A, 6B and 6B2.

Tracer	Matrix sorption coefficient K_d (m^3/kg)	Surface sorption coefficient K_a (m)	Effective matrix diffusivity D_e (m^2/s)
I	0		6.23E-14
Sr	7.75E-5*)		3.00E-14
Co	2.50E-3*)		2.18E-14
Tc	0.2**)		3.00E-14
Am	0.5**)		3.00E-14

*) from Byegård *et al*., 2001
**) from Selroos J-O *et al*., 2001

Table 3-6. Sorption and diffusivity data for tracers in gouge for Task 6A, 6B and 6B2.

Tracer		Matrix sorption coefficient K_d (m^3/kg)	Surface sorption coefficient K_a (m)	Effective matrix diffusivity D_e (m^2/s)
I		0		
Sr		1.98E-4*)		
Co		1.20E-2*)		
Tc	Case 1	0.2		
	Case 2	2.0		
Am	Case 1	0.5		
	Case 2	5.0		

*) calibrated through simulations for STT-1b tests

Table 3-7. Transmissivities at borehole sections identified on basis of drawdowns at borehole sections during tracer tests.

Borehole Section	Transmissivity (m^2/s)
KXTT1 R2	$9.68 \cdot 10^{-9}$
KXTT2 R2	$3.45 \cdot 10^{-9}$
KXTT3 R2	$4.14 \cdot 10^{-3}$
KXTT4 R3	$2.87 \cdot 10^{-8}$
KA3005A R3	$4.20 \cdot 10^{-8*}$

* Not identified but determined from flow- and pressure build-up tests

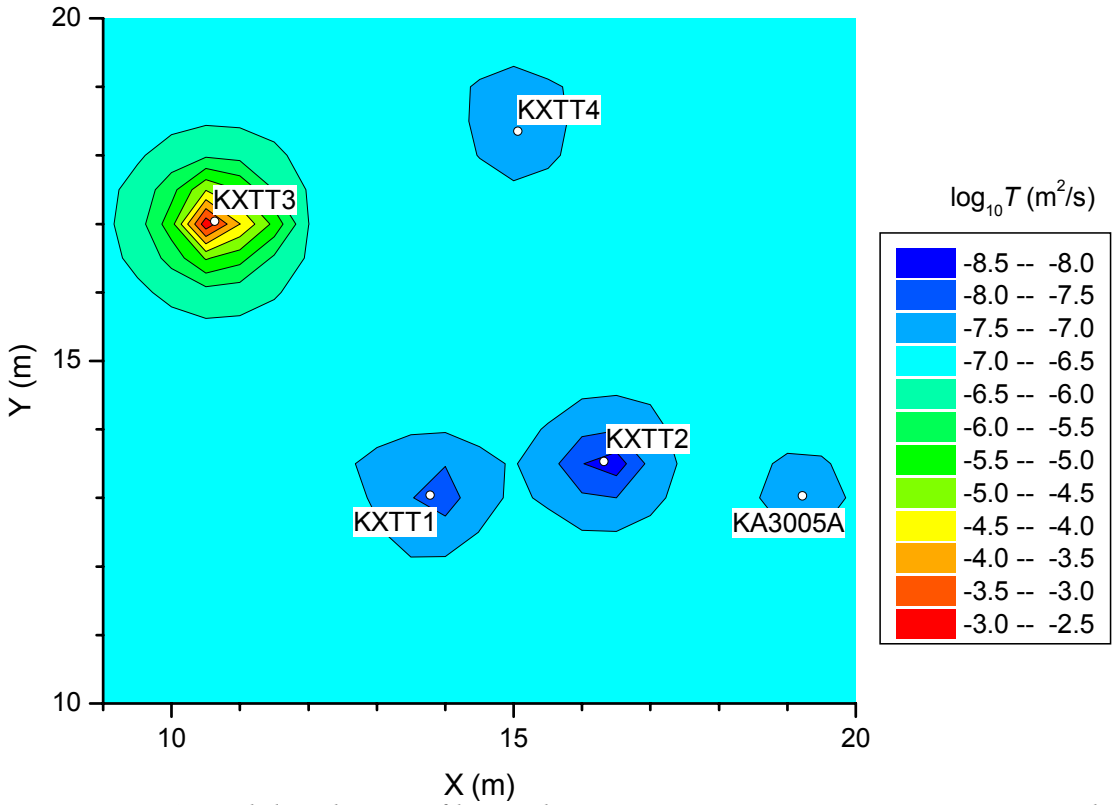

Figure 3-5. *Spatial distribution of logarithmic transmissivitiy in Feature A estimated by kriging on basis of the identified transmissivities at the five borehole sections. (KXTT1 R2:(X,Y)=(13.78, 13.04), KXTT2 R2:(16.32, 13.53), KXTT3 R2:(10.63, 17.04), KXTT4 R3:(15.06, 18.35), KA3005A R3:(19.22, 13.03))*

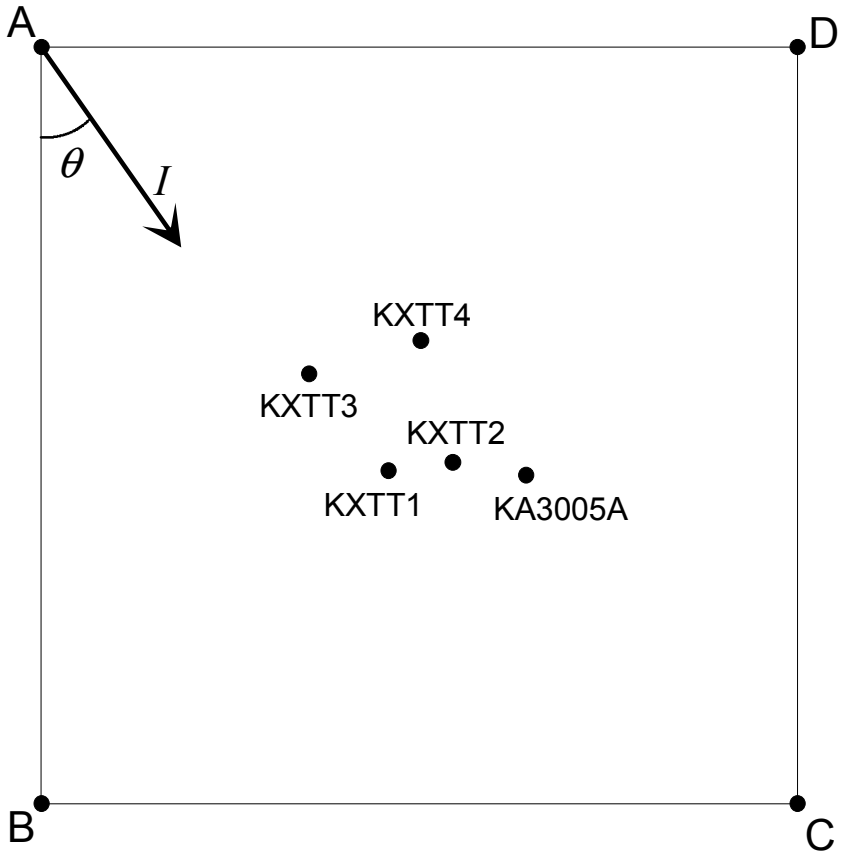

Figure 3-6. *Schematic diagram for parameters defining hydraulic boundary conditions.*

Table 3-8. Identified values of parameters for hydraulic boundary conditions.

Parameters	RC-1
Hydraulic head, h_A	-52.7 mH_2O
Magnitude of hydraulic gradient, I	0.164
Direction of hydraulic gradient, θ	56.7°

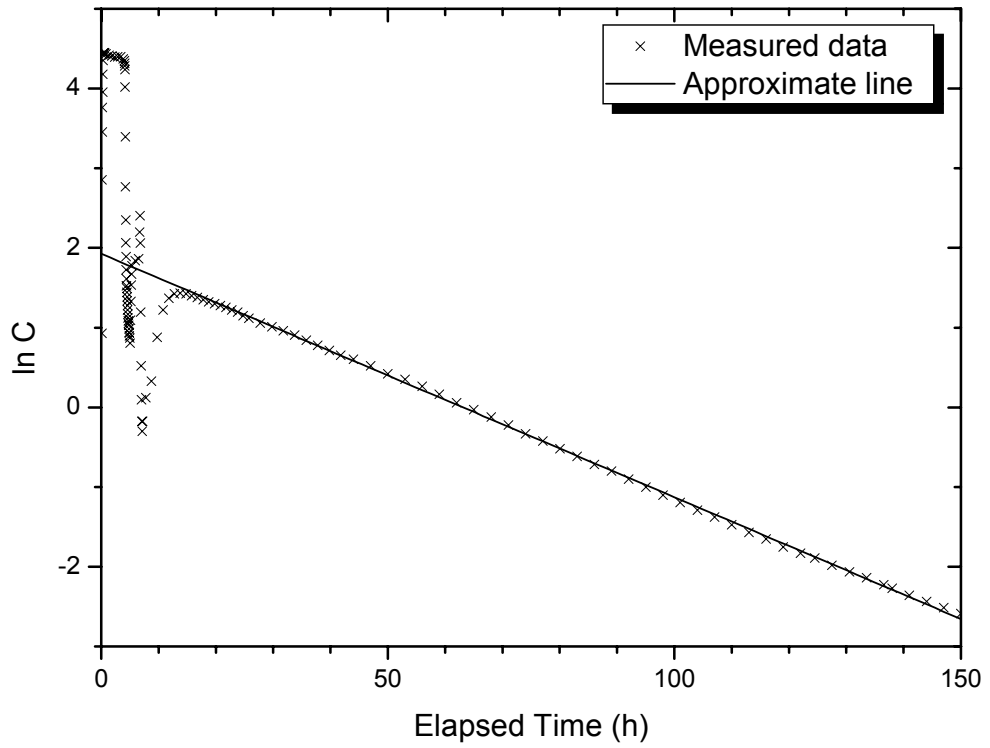

Figure 3-7. *Injected concentration of Uranine (ln C) in KXTT1 R2 during STT-1b.*

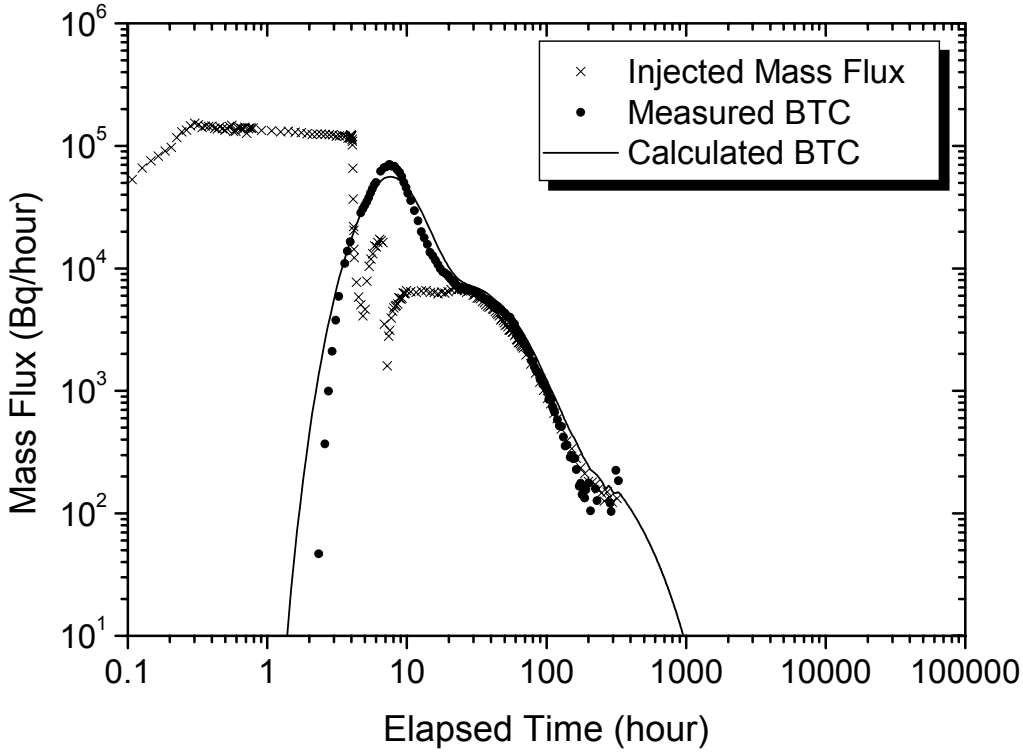

Figure 3-8. *Measured breakthrough curve of I-131 in pumping section during STT-1b and result of the best-fit run.*

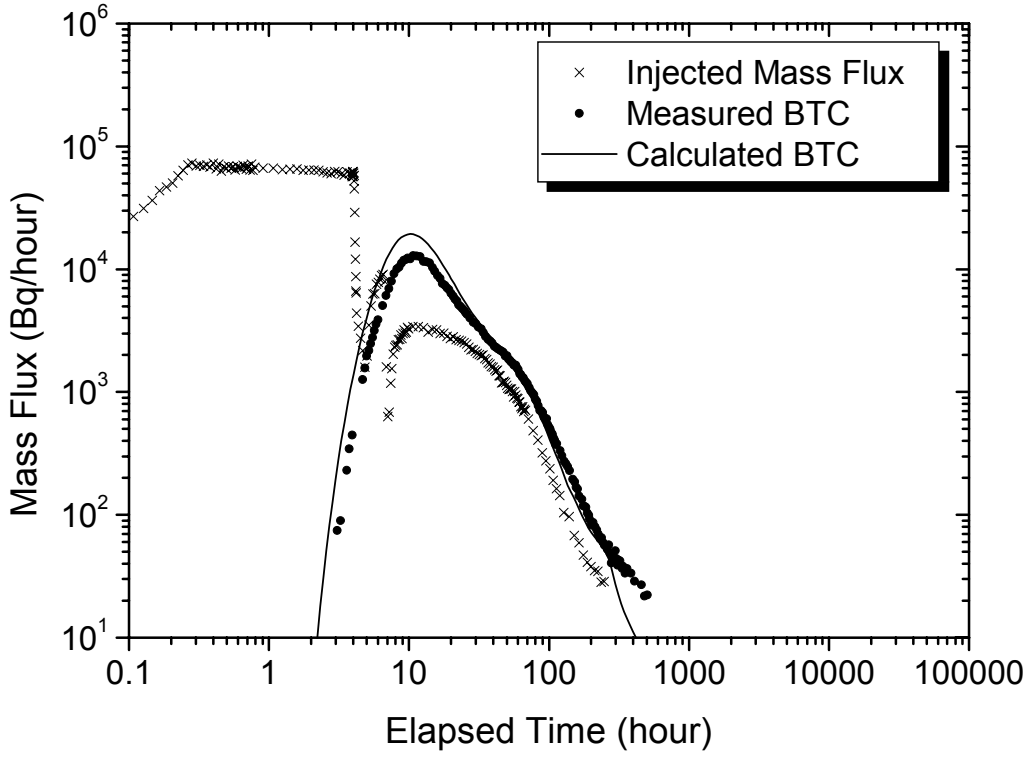

Figure 3-9. *Measured breakthrough curve of Sr-85 in pumping section during STT-1b and result of the best-fit run.*

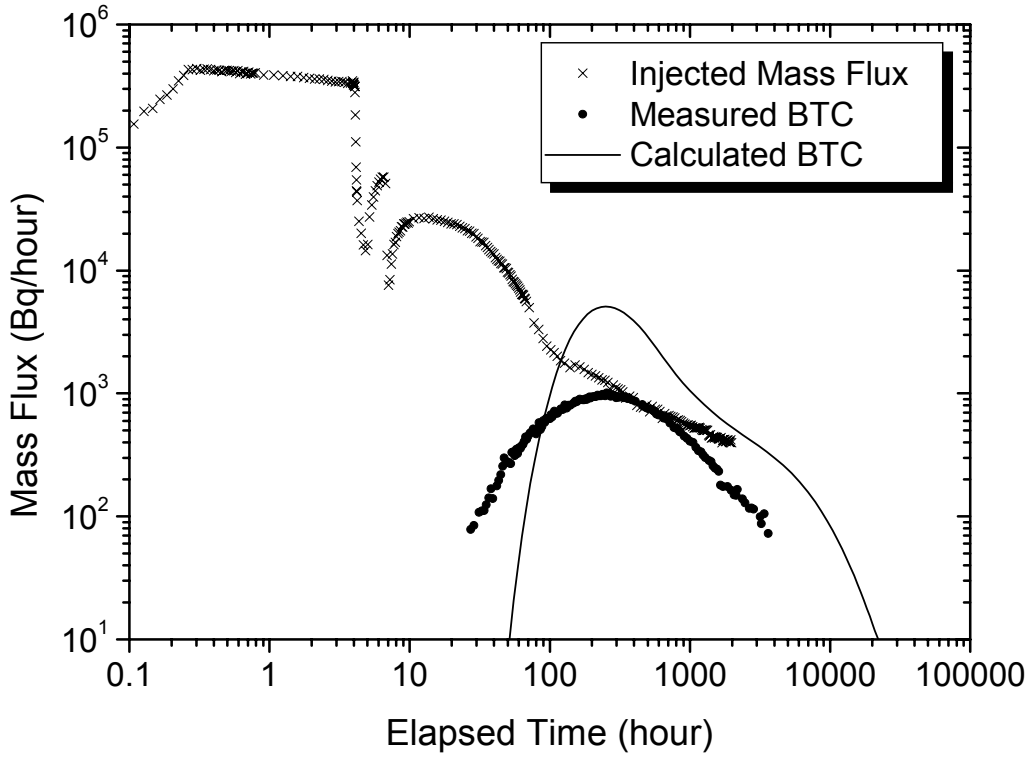

Figure 3-10. *Measured breakthrough curve of Co-58 in pumping section during STT-1b and result of the best-fit run.*

4 Results - Performance measures

4.1 Task 6A

At first, groundwater flow in Feature A and the surrounding rock matrix during STT-1b was calculated. Next a numerical analysis for tracer migration was performed for the measured injection curves of STT-1b. The tracers modelled in the analysis were americium as well as iodine, strontium, cobalt and technetium that were actually used in STT-1b. Furthermore the migration of tracers was simulated for Dirac pulse injection under the same condition of groundwater flow as STT-1b.

4.1.1 Drawdown in injection and pumping borehole

The measured and calculated values of drawdown and hydraulic head at the borehole sections during STT-1b are shown in Table 4-1. The calculated hydraulic head at the pumping section, KXTT3 R2, agrees well with the measured one. But the calculated hydraulic head at the tracer injection section, KXTT1 R2, is 3.1 meters lower than the measured one. Therefore the calculated head difference between those two sections is smaller than the measured one.

4.1.2 Breakthrough time history for the tracers

The breakthrough curves at the pumping section for the measured injection curves of STT-1b and Dirac pulse injection are shown in Figure 4-1 and Figure 4-2, respectively. And the breakthrough times for recovery of 5, 50 and 95% of the injected mass in STT-1b and the Dirac pulse injection are shown in Table 4-2 and Table 4-3, respectively. In the simulation for the Dirac pulse injection, it was assumed that the unit quantity of tracer was injected in 10 minutes. The more strongly adsorptive the tracer was, the slower its breakthrough time was. The breakthrough time for recovery of 50 %, t_{50}, of the pulse injection of the non-sorbing tracer, iodine, was $1.95 \cdot 10^{-3}$ years after the tracer test began. On the other hand, t_{50} of the most strongly adsorptive tracer, americium, was 3.64 years after, even in the Case 1 where its adsorptivity was set weaker than in Case 2. The finish time of calculation was 10 years after the tracer test began and at the time the total recovery rates of the strongly adsorptive tracers, technetium and americium, were below 95 %.

4.1.3 Maximum release rate

The maximum release rate using measured injection curves of STT-1b and the Dirac pulse injection are shown in Table 4-4 and Table 4-5, respectively. The more strongly adsorptive the tracer was, the smaller its maximum release rate was. The maximum release rate of the non-sorbing tracer, iodine, was $1.08 \cdot 10^{3}$ year^{-1}. On the other hand, the maximum release rate of the most strongly adsorptive tracer, americium was only $6.19 \cdot 10^{-2}$ year^{-1} in the Case 2 where its adsorptivity was set stronger than in Case 1. The maximum release rate of the pulse injection of iodine was $1.74 \cdot 10^{4}$ larger than the one in the Case 2 of americium.

4.2 Task 6B

At first, groundwater flow in Feature A and the surrounding rock matrix was calculated at the pumping rate of 0.1 % of STT-1b. Next a numerical analysis for tracer migration was performed for the constant injection rate and a Dirac pulse injection, respectively. The tracers modelled in the analysis were the same as in Task 6A.

4.2.1 Breakthrough time history for the tracers

The calculated head differnce between the pumping and tracer injection sections was 0.0079 mH_2O. As a result, the proportion of the hydraulic gradient between the them in Task 6B to the one in Task 6A was 0.105 %.

The breakthrough curves at the pumping section for the constant injection rate and a Dirac pulse injection are shown in Figure 4-3 and Figure 4-4, respectively. And the breakthrough times for recovery of 5, 50 and 95% of a Dirac pulse injection are shown in Table 4-6. The breakthrough time for recovery of 50 %, t_{50}, of the pulse injection of the non-sorbing tracer, iodine, was 0.93 years after the tracer test began. On the other hand, t_{50} of the most strongly adsorptive tracer, americium, was $2.14 \cdot 10^4$ years after in the Case 2 where its adsorptivity was set stronger than in Case 1. The finish time of calculation was 10^7 years after the tracer test began and at the time the total recovery rate of only americium was below 95 %.

4.2.2 Maximum release rate

The maximum release rates using a Dirac pulse injection are shown in Table 4-7. The maximum release rate of the non-sorbing tracer, iodine, was 0.88 $year^{-1}$. On the other hand, the maximum release rate of the most strongly adsorptive tracer, americium was only $3.74 \cdot 10^{-5}$ $year^{-1}$ in the Case 2 where its adsorptivity was set more strongly. The maximum release rate of iodine was $2.35 \cdot 10^4$ larger than the one in the Case 2 of americium.

The proportion of the maximum release rate in Task 6B to the one in Task 6A was smaller than the proportion of hydraulic gradient and was the largest, 0.08 %, in iodine and the smallest, 0.035 %, in the Case 1 of technetium.

4.3 Task 6B2

At first, groundwater flow in Feature A and the surrounding rock matrix was calculated in case of an overall hydraulic gradient of 0.1 % between the two intersecting fractures. Next a numerical analysis for tracer migration was performed for the constant injection rate and a Dirac pulse injection, respectively. In the tracer migration analysis, not only a 3-D model but also a 1-D model were used. The tracers modelled in the analysis were the same as in Task 6A and Task 6B.

4.3.1 Breakthrough time history for the tracers

The breakthrough curves at the Fracture Y for the constant injection rate and a Dirac pulse injection are shown in Figure 4-5 and Figure 4-6, respectively. And the breakthrough times for recovery of 5, 50 and 95% of a Dirac pulse injection are shown in Table 4-8. When a three-dimensional model was used, the breakthrough time for recovery of 50 %, t_{50}, of the pulse injection of the non-sorbing tracer, iodine, was 1.91 years after the tracer test began and t_{50} of the most strongly adsorptive tracer, americium, was $5.5 \cdot 10^4$ years after in the Case 2 where its adsorptivity was set stronger than in Case 1. On the other hand, when a one-dimensional model was used, t_{50} of iodine and americium in Case 2 were 1.33 years and $1.78 \cdot 10^4$ years after, respectively.

4.3.2 Maximum release rate

The maximum release rates using a Dirac pulse injection are shown in Table 4-9. When a three-dimensional model was used, the maximum release rate was the largest, $4.28 \cdot 10^{-1}$ year^{-1}, in iodine and the smallest, $1.51 \cdot 10^{-5}$ year^{-1}, in the Case 2 of americium. On the other hand, when a one-dimensional model was used, the maximum release rate was the largest, $7.84 \cdot 10^{-1}$ year^{-1}, in iodine and the smallest, $5.71 \cdot 10^{-5}$ year^{-1}, in the Case 2 of americium.

Table 4-1. Measured and calculated values of drawdown and hydraulic head at borehole sections during the tracer test, STT-1b.

Borehole Section	Drawdowns (m)		Hydraulic heads (m)	
	Measured	Calculated	Measured	Calculated
KXTT1 R2	4	7.1	-57.02	-60.10
KXTT2 R2	12	5.4	-65.03	-58.60
KXTT3 R2	15	15.0	-67.62	-67.60
KXTT4 R3	2.4	7.5	-55.28	-60.35
KA3005A R3	2.3	3.4	-55.87	-56.87

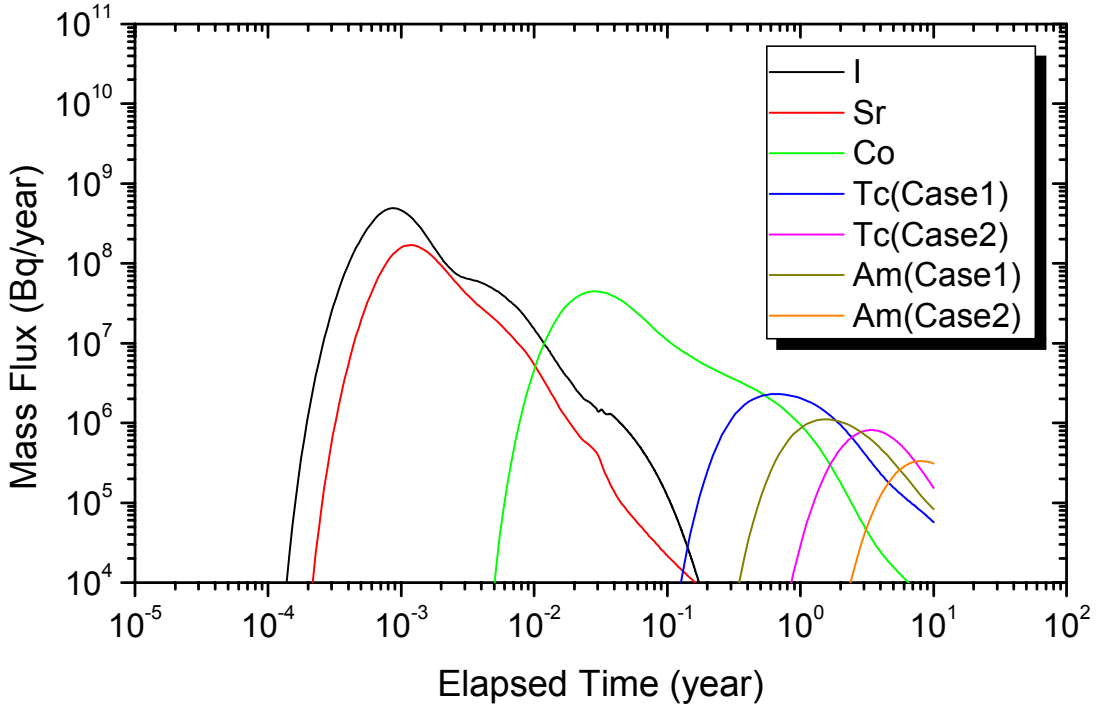

Figure 4-1. *Breakthrough curves at the pumping section for measured injection curves of STT-1b.*

Table 4-2. Breakthrough times for recovery of 5, 50 and 95% of the injected mass of STT-1b.

Tracer	t_5 (year)	t_{50} (year)	t_{95} (year)
I	6.05E-04	1.95E-03	3.13E-02
Sr	7.99E-04	2.16E-03	1.66E-02
Co	2.17E-02	1.60E-01	2.03E+00
Tc_Case 1	4.32E-01	1.82E+00	-
Tc_Case 2	2.10E+00	5.65E+00	-
Am_Case 1	1.03E+00	4.01E+00	-
Am_Case 2	5.06E+00	-	-

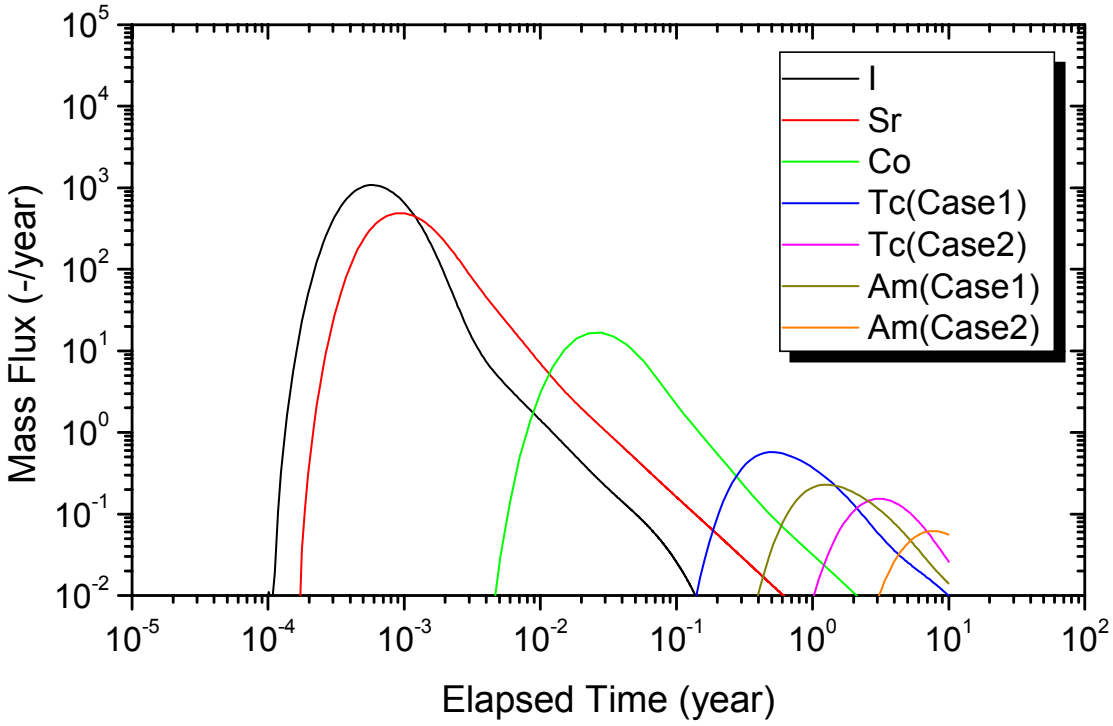

Figure 4-2. *Breakthrough curves at the pumping section for the Dirac pulse injection under the same condition of groundwater flow as STT-1b.*

Table 4-3. Breakthrough times for recovery of 5, 50 and 95% of the Dirac pulse injection under the same condition of groundwater flow as STT-1b.

Tracer	t_5 (year)	t_{50} (year)	t_{95} (year)
I	3.54E-04	8.22E-04	2.58E-03
Sr	5.94E-04	1.67E-03	3.36E-02
Co	1.60E-02	4.75E-02	5.00E-01
Tc_Case 1	3.60E-01	1.46E+00	-
Tc_Case 2	1.94E+00	5.32E+00	-
Am_Case 1	8.98E-01	3.64E+00	-
Am_Case 2	4.85E+00	-	-

Table 4-4. Maximum release rate using measured injection curves of STT-1b.

Tracer	Max. release rate (Bq/year)
I	4.92E+8
Sr	1.70E+8
Co	4.47E+7
Tc_Case 1	2.31E+6
Tc_Case 2	8.15E+5
Am_Case 1	1.11E+6
Am_Case 2	3.34E+5

Table 4-5. Maximum release rate using Dirac pulse injection under the same condition of groundwater flow as STT-1b.

Tracer	Max. release rate (-/year)
I	1.08E+3
Sr	4.90E+2
Co	1.68E+1
Tc_Case 1	5.74E-1
Tc_Case 2	1.53E-1
Am_Case 1	2.29E-1
Am_Case 2	6.19E-2

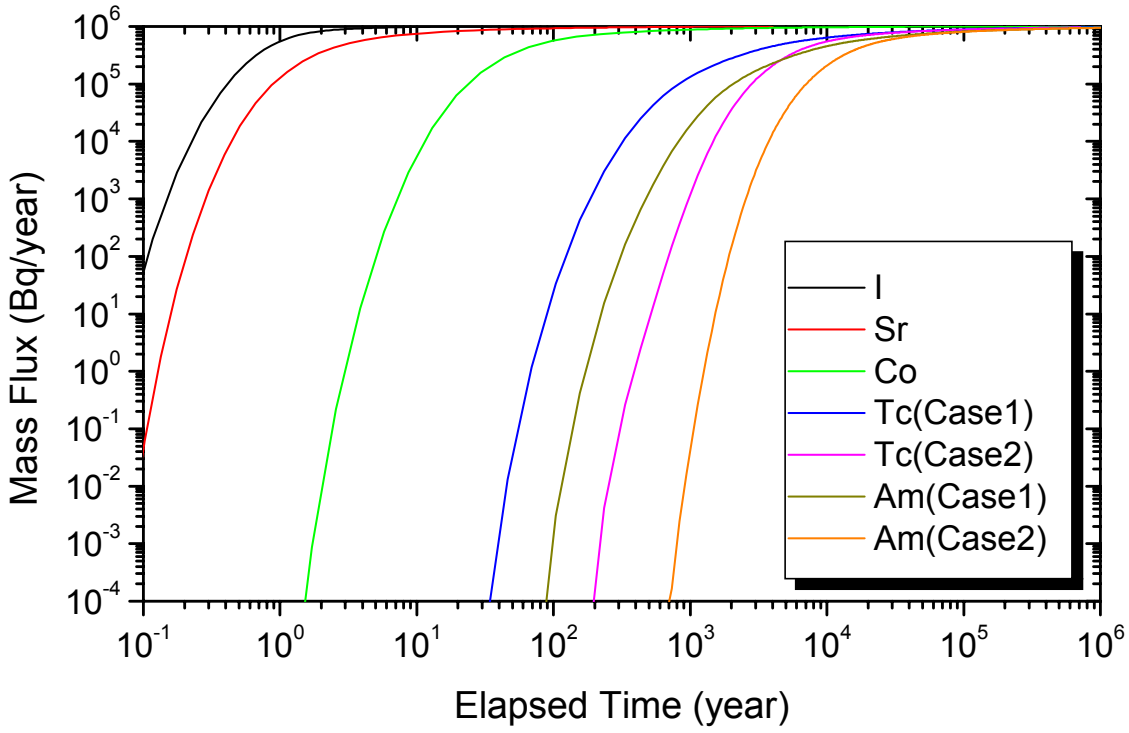

Figure 4-3. *Breakthrough curves for constant injection rate in Task 6B.*

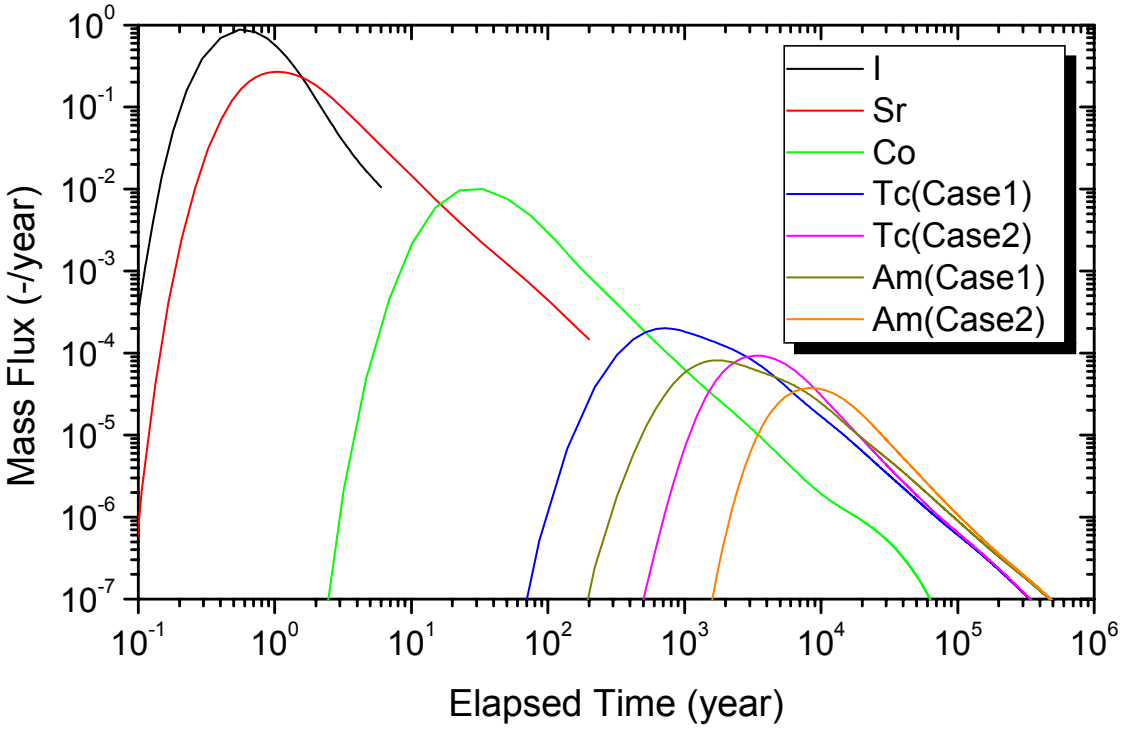

Figure 4-4. *Breakthrough curves for Dirac pulse injection in Task 6B.*

Table 4-6. Breakthrough times for recovery of 5, 50 and 95% of the Dirac pulse injection in Task 6B.

Tracer	t5 (year)	t_{50} (year)	t_{95} (year)
I	3.40E-1	9.30E-1	4.47E+0
Sr	6.90E-1	2.99E+0	6.54E+1
Co	1.83E+1	7.74E+1	1.26E+3
Tc_Case 1	5.88E+2	4.87E+3	4.07E+5
Tc_Case 2	2.22E+3	8.60E+3	4.13E+5
Am_Case 1	1.45E+3	1.21E+4	-
Am_Case 2	5.56E+3	2.14E+4	-

Table 4-7. Maximum release rate using Dirac pulse injection in Task 6B.

Tracer	Max. release rate (-/year)
I	8.80E-1
Sr	2.69E-1
Co	9.99E-3
Tc_Case 1	2.01E-4
Tc_Case 2	9.29E-5
Am_Case 1	8.17E-5
Am_Case 2	3.74E-5

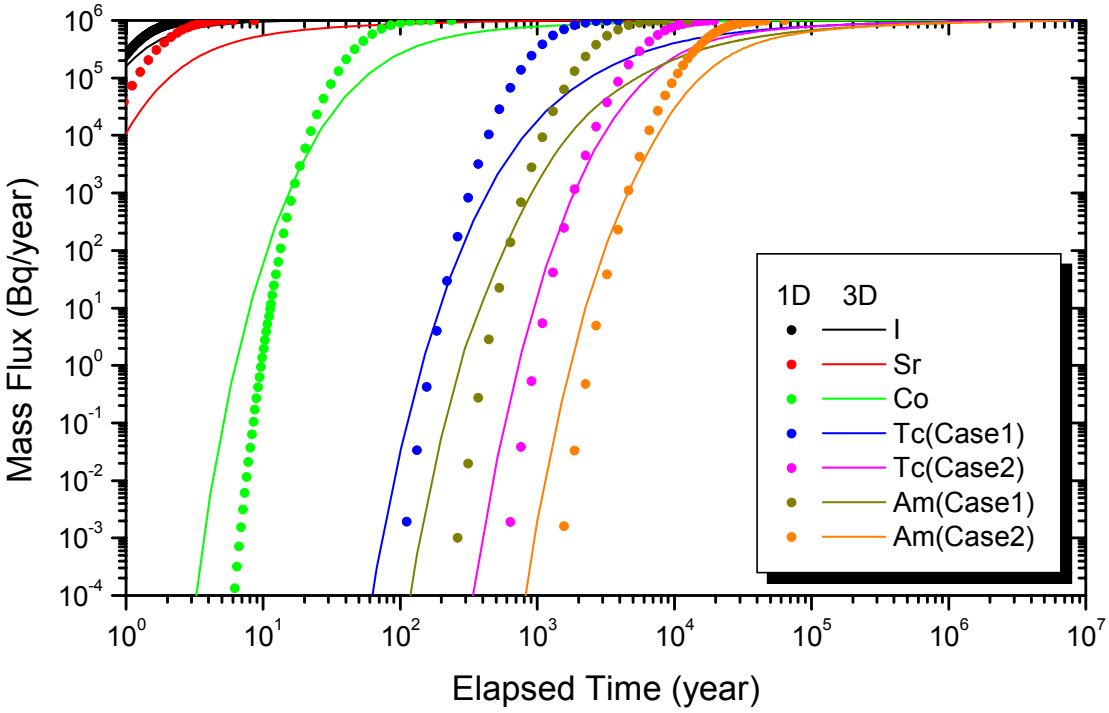

Figure 4-5. *Breakthrough curves for constant injection rate in Task 6B2.*

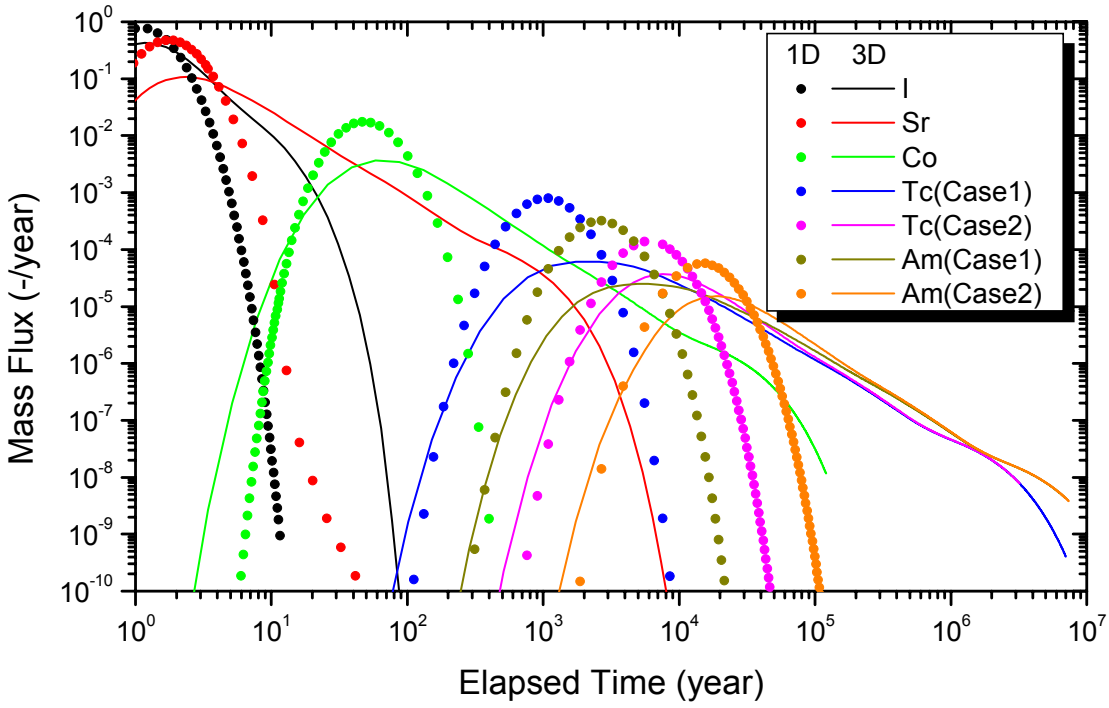

Figure 4-6. *Breakthrough curves for Dirac pulse injection in Task 6B2.*

Table 4-8. Breakthrough times for recovery of 5, 50 and 95% of the Dirac pulse injection in Task 6B2.

Tracer	t_5 (year)		t_{50} (year)		t_{95} (year)	
	3D	1D	3D	1D	3D	1D
I	7.04E-1	6.73E-1	1.91E+0	1.33E+0	6.72E+0	2.62E+0
Sr	1.58E+0	1.03E+0	7.84E+0	2.12E+0	1.18E+2	4.17E+0
Co	4.32E+1	2.87E+1	2.32E+2	5.83E+1	1.33E+4	1.11E+2
Tc_Case 1	1.62E+3	6.03E+2	1.45E+4	1.26E+3	3.69E+5	2.42E+3
Tc_Case 2	4.99E+3	3.47E+3	2.22E+4	7.30E+3	4.78E+5	1.45E+4
Am_Case 1	4.00E+3	1.51E+3	3.63E+4	3.15E+3	9.89E+5	6.05E+3
Am_Case 2	1.24E+4	8.74E+3	5.50E+4	1.78E+4	1.19E+6	3.53E+4

Table 4-9. Maximum release rate using Dirac pulse injection in Task 6B2.

Tracer	3D-model (-/year)	1D-model (-/year)
I	4.28E-1	7.84E-01
Sr	1.07E-1	4.74E-01
Co	3.67E-3	1.75E-02
Tc_Case 1	6.12E-5	7.96E-04
Tc_Case 2	3.69E-5	1.37E-04
Am_Case 1	2.49E-5	3.19E-04
Am_Case 2	1.51E-5	5.71E-05

5 Discussion

5.1 Conceptual issues

In Task 6A, the recovered mass flux decreased more rapidly after the peak than in Task 6B and 6B2. So relatively advection was prominent in Task 6A and matrix diffusion was prominent in Task 6B and 6B2. The significant technical issues in achieving Task 6A were estimation of transmissivity distribution and aperture of Feature A and sorption coefficients in gouge. On the other hand, the significant technical issues in achieving Task 6B and6B2 were estimation of sorption coefficients in altered rim and intact rock.

We think that there is no particular problem in the conventional advection-dispersion-diffusion (ADD) approach and the problem is how we can estimate the geological structure and the values of input parameters accurately.

5.2 Lessons learned

In order to improve the reliability of a performance assessment, it is very important how to estimate accurately the transport properties, especially surface and matrix sorption coefficients, from the results of in-situ tracer experiments and laboratory tests. And we need to take the irreversible adsorption process into consideration to predict the migration of some radionuclides such as cobalt.

In this study, the breakthrough curves obtained by using the one-dimensional model were very different from the ones by using the three-dimensional model. In case of performing a performance assessment by using a one-dimensional model, it is one of the significant problems to be solved how to find the value of dispersion length that produces the same calculated result as a three-dimensional model.

6 References

Swedish Nuclear Fuel and Waste Management Co. (SKB), 2003. ÄspöHard Rock Laboratory, Planning Report for 2003. SKB International Progress Report IPR 03-24.

Selroos J-O, Elert M, 2001. TASK 6A & 6B Modeling task specification Version 1.0.

Elert M, Selroos J-O, 2001. TASK 6B2 Modeling task specification Version 1.0.

Kawanishi M, Igarashi T, Mahara Y, Komada H, Maki Y, 1987. Computer models for safety assessment on land disposal of low-level wastes. Waste Management '87, 3, Tucson, Arizona, pp. 175-180.

Yeh G T *et al*., 1979. FEMWATER. A finite-element model of water flow through saturated-unsaturated porous media. ORNL-5567.

Yeh G T *et al*., 1981. FEMWASTE. A finite-element model of waste transport through saturated-unsaturated porous media. ORNL-5601.

Winberg A, Andersson P, Hermanson J, Byegård J, Cvetkovic V, Birgersson L, 2000. Äspö Hard Rock Laboratory, Final report of the first stage of the tracer retention understanding experiments, Swedish Nuclear Fuel and Waste Management Co, TR-00-07.

Byegård J, Widestrand H, Skålberg M, Tullborg E-L, Siitari-Kauppi M, 2001. Complementary investigations of diffusivity, porosity and sorptivity of Feature A - site specific material, ICR-01-04, Swedish Nuclear Fuel and Waste Management Co, Stockholm, Sweden.

Delhomme J P, 1976. Application de la théorie des variables régionalisées dans les sciences de l'eau. Thèse, Univ. Paris VI.

Abelin H, Birgersson L, Widen H, Ågren T, 1990. Channeling experiment. OECD/NEA International Stripa Project. Stripa Technical Report TR 90-13.

Winberg A, 1996. Descriptive structural-hydraulic models on block and detailed scales of the TRUE-1 site. SKB International Cooperation Report ICR 94-08.

Andersson P, 1996, TRUE 1st stage tracer test program. Experimental data and preliminary evaluation of the TRUE-1 radially converging tracer test (RC-1). Äspö Hard Rock Laboratory Progress Report HRL-96-24.